Supplementary Material

Supplementary Material to:
Revisiting the Contemporary Sea Level Budget on Global and Regional Scales
Authors:
Roelof Rietbroek, Sandra-Esther Brunnabend, Jürgen Kusche, Jens Schröter, Christoph Dahle
The data used for this paper can be downloaded from the Pangaea Archive:
http://dx.doi.org/10.1594/PANGAEA.855539

Joint inversion weighting scheme

For completeness we describe here how the different datasets are combined in the joint inversion (see also [1]).

Altimetry
For each month we create for every altimetry satellite a normal equation system:

$$N_{Jasonx}(t)\,\mathbf{x}(t) = \mathbf{b}_{Jasonx}(t)\,,\ _{x=1,2} \tag{s1}$$

The to-be-solved-for solution vector $\mathbf{x}$ contains vectors of the individual elements:

$$\mathbf{x} = \begin{bmatrix} x_{ice} \\ x_{glac} \\ x_{hydro} \\ x_{gia} \\ x_{steric} \\ x_{other} \\ x_{satbias} \end{bmatrix} \tag{s2}$$

The normal matrix, N_{Jasonx}, can be computed from the observation equation (equation 1 from the main paper) as:

$$N_{Jasonx}(t) = \begin{bmatrix} B^T Y^T & C^T K^T \end{bmatrix} C^{-1}_{Jasonx}(t) \begin{bmatrix} YB \\ KC \end{bmatrix} \tag{s3}$$

Where we use a diagonal error-covariance matrix, C_{Jasonx}, which is constructed from the range errors provided by the radar altimeters (derived from the noise of the 20Hz data).

The right hand side of the normal equation system is computed as:

$$\mathbf{b}_{Jasonx}(t) = \begin{bmatrix} B^T Y^T & C^T K^T \end{bmatrix} C^{-1}_{Jasonx}(t) \left(\delta h^{Jasonx}_{sla}(t,\theta,\lambda) - OBP^*_{GAC}(\theta,\lambda) \right) \tag{s4}$$

The sea level anomalies were already corrected with a high frequency (< 10days) dynamic atmospheric correction (DAC), but we additionally reduce the signal for monthly averages of our Ocean Atmosphere correction (see equation 3 of the main article), in order to be consistent with the GRACE processing.

GRACE
The GRACE data is provided in terms of normal equation systems, expressed in normalized Stokes coefficients. From the systems we eliminate (i.e. solve implictly [2]) auxiliary parameters, such as initial orbit state vectors, and accelerometer scales, until we are left with a system which is linked to the vector of monthly Stokes coefficients, $\phi_{nm}(t)$ up to degree and order 150:

$$N_{\phi}(t)\,\phi_{nm}(t) = \mathbf{b}_{\phi}(t) \tag{s5}$$

The signal in this system of equation is already reduced with the standard GRACE dealiasing product, but also with trends, and (semi)annual harmonics derived from the EIGEN-6c static gravity field model. To make the data consistent with altimetry we therefore need to apply a small update to the right hand side vector of the system:

$$\mathbf{b}^*_{\phi} = \mathbf{b}_{\phi} - N_{\phi}\delta\phi_{nm}(t) \tag{s6}$$

The update vector $\delta\phi_{nm}(t)$ contains Stokes coefficients with a contribution from the ocean mean of the monthly GAC product (right hand side of equation 3 of the main article), and an additional component which is used to restore the time variable part of the EIGEN-6c model.

This system can now be transformed into a system expressed in our parameters of interest $\mathbf{x}$ by:

$$N_{GRACE}(t) \begin{bmatrix} x_{ice} \\ x_{glac} \\ x_{hydro} \\ x_{gia} \end{bmatrix} = \mathbf{b}_{GRACE}(t) \tag{s7}$$

Where we use the observation equation 2 from the main article to convert the normalmatrix and right hand side:

$$N_{GRACE}(t) = B^T N_{\phi} B \tag{s8}$$

$$\mathbf{b}_{GRACE}(t) = B^T \mathbf{b}^*_{\phi} \tag{s9}$$

Variance Component Estimation
When combining normal equation systems from GRACE and altimetry we allow their error-covariance to be scaled by a scalar variance component. This will absorb systematic over- or underestimation of the formal error covariance, which may occur in different observation techniques.

$$N_{comb}(t) = \frac{1}{\sigma^2_{GRACE}} N_{GRACE} + \frac{1}{\sigma^2_{Jason1}} N_{Jason1} + \frac{1}{\sigma^2_{Jason2}} N_{Jason2} \tag{s10}$$

$$\mathbf{b}_{comb}(t) = \frac{1}{\sigma^2_{GRACE}} \mathbf{b}_{GRACE} + \frac{1}{\sigma^2_{Jason1}} \mathbf{b}_{Jason1} + \frac{1}{\sigma^2_{Jason2}} \mathbf{b}_{Jason2} \tag{s11}$$

In this study we estimate the variance components σ^2 iteratively according to [3].

Solution of common parameters
The common parameters, are those which need to be solved using the full length of the series (e.g. x_{gia} and $x_{satbias}$). These can be solved by eliminating (i.e. solve implicitly) the time-variable parameters from all the monthly normal equation systems, and aggregating all of them into a single one:

$$N_{com} \begin{bmatrix} x_{gia} \\ x_{satbias} \end{bmatrix} = \mathbf{b}_{com} \tag{s12}$$

This system is then solved for the x_{gia} and $x_{satbias}$.

Solution of the monthly parameters
Using the estimated common parameters, we can update each monthly normal equation system, and subsequently remove (do not solve implicitly) the GIA and bias parameters. This two step approach, utilizes the uncorrelatedness of the different normal equation systems, and results in the same set of estimated parameters as if the entire system (all monthly and common parameters from all data) would have been solved in a single step[1].

Fingerprints of Ice Sheets, Glaciers and Hydrology

The Greenland and Antarctica ice sheets are discretized in 16 and 27 drainage basins (see Fig. S1), as described in [4, 5]. Over the ocean, we compute the response of the geoid to a uniform layer of 1Gt in the basin, augmenting it by a uniform shift to ensure mass conservation. The procedure, generally known as 'solving the sea level equation' is performed in the spectral domain [6], and accounts for rotational feedback. The combined effect of the basin load and the ocean, covers the entire globe and is consistent in terms of gravity, surface deformation and mass. For each basin, we now obtain two independent observables: the shifted geoid (geocentric sea level) and the associated elastic crustal deformation. From those we can trivially derive other observables, such as gravitational potential changes and relative sea level. For a constant ocean function, appropriate for the period considered here, the sea level equation is linear allowing a superposition of different contributions, conserving mass and yielding a consistent gravity and deformation response.

The construction of fingerprints for the land glaciers follows the same procedure, except that the ice load of the drainage basins are replaced by 16 clusters of glaciers (see Fig. S1). Glacier positions are taken fom the WGI/GLIMS database [7], and are grouped per region.

Another important mass signal originates from terrestrial variations in hydrology. We have analyzed monthly grids of total water storages from the WaterGap Global Hydrology Model (WGHM)[8], and took the first 60 leading EOF's as fingerprints. These modes explain more than 99% of the model variance, and are therefore adequate to capture a wide range of different hydrological signals. In the EOF analysis we discarded cells which were in glacier regions, and on Greenland. Again, a consistent passive sea level response over the ocean was computed for each mode with the procedure above.

Glacial Isostatic Adjustment
Modelling the gravity and sea level signals of glacial isostatic adjustment has been recognized as a major source of error in closing the sea level budget [9]. Therefore, we have chosen to represent the GIA signal by 5 complementary patterns, and adjust these within the inversion. To parameterize the GIA signal, we used modelling results from [10], who used a visco-elastic Earth model (VM2), and forced it with the ice loading history ICE-5G [11], augmented with a loading history in Greenland. Besides this reference run, different runs were produced in which the ocean coastline remained fixed but 5 different melting sources (Laurentide, Fennoscandia, Antarctica, Greenland, and the

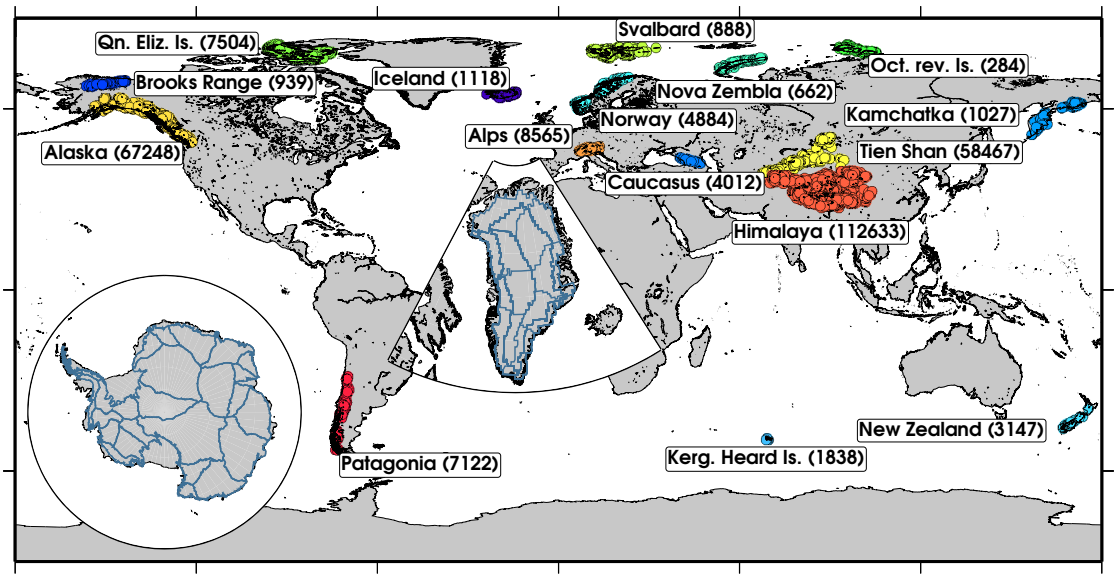

Figure S1: Overview of the used glacier clusters (numbers in between brackets are the amount of point loads per cluster) and ice sheet delineation

remainder of the load) were allowed to vary. For present day rates, the 5 different contributions approximately add up to the reference run, and can therefore be used to parameterize the GIA signal. A priori, we correct the GRACE and altimetry data with the reference run. In the inversion step, we subsequently estimate 5 different source corrections to the reference model, in order to absorb GIA-model deficiencies. The estimation of the GIA parameters is ill-posed and requires a stabilization (see the paragraph on stabilization below). The estimated GIA parameters and their effect on global mean sea level are tabulated in table S1 and S2.

Steric and Auxiliary Fingerprints

Steric changes in the ocean were computed by integrating salinity and temperature induced volume changes from the Finite Element Sea Ice Model (FESOM). The first 200 EOFs, accounting for more then 99% of the modelled steric height variances, were then used to parameterize the steric changes.

After an initial inversion, it turned out that still significant large scale non-stochastic signal exists in the altimetry residuals (see Fig. S2). For this reason, a second set of patterns have been constructed. These have been computed as follows: after the initial inversion, the altimetric height residuals have been gridded and consequently smoothed by a 200km Gaussian filter (the high resolution signal is not of interest here). An additional EOF analysis has been applied to these smoothed grids and the first 100 EOFs (explaining more than 97% of the smoothed residuals) are now used as additional fingerprints in the inversion. The use of those additional fingerprints absorb a significant part of the altimetry residuals as can be seen from Fig. S2.

During the review of a previous version of this paper, concerns arose about the sensitivity of the inversion results to the chosen steric parameterization. To illustrate the effect of the chosen steric patterns, we have constructed an additional inversion, where we used patterns obtained from the steric heights computed from the gridded Ishii data (first 1500m) [12]. For this inversion we've used a dedicated set of auxiliary patterns computed from the residuals. Similar to figure 2 of the main article, the associated global and regional sea level budget is depicted in figure S3. It can be observed that the combined total trends only change within the errorbars. Interesting is to see that more signal is absorbed in the global mean steric trend when using the steric patterns derived from the FESOM model. Only 1.2±0.3 mm/yr (versus 1.4±0.16 mm/yr) of the steric trend can be explained when using the patterns from the Ishii data. On regional scales, there may be regions where the patterns from the Ishii data may perform better (for example in the Mediterranean, where the discretization of FESOM may not be sufficiently dense). However, in the current paper we decided to stick with the patterns from FESOM as it provides estimates which are entirely independent on the ARGO data and cover the full ocean column.

Furthermore, we would like to emphasize that the applied inversion scheme results in steric changes which are significantly different from that of the FESOM model itself. This is illustrated in S4, where the first 8 estimated principal components (explaining 81% of the model variance), are compared with the PC's as computed from the model. For comparison, the steric heights from the the Ishii data [12], are projected on the same EOF's and are also plotted. It can be seen that the estimated PC's from the inversion differ significantly from the

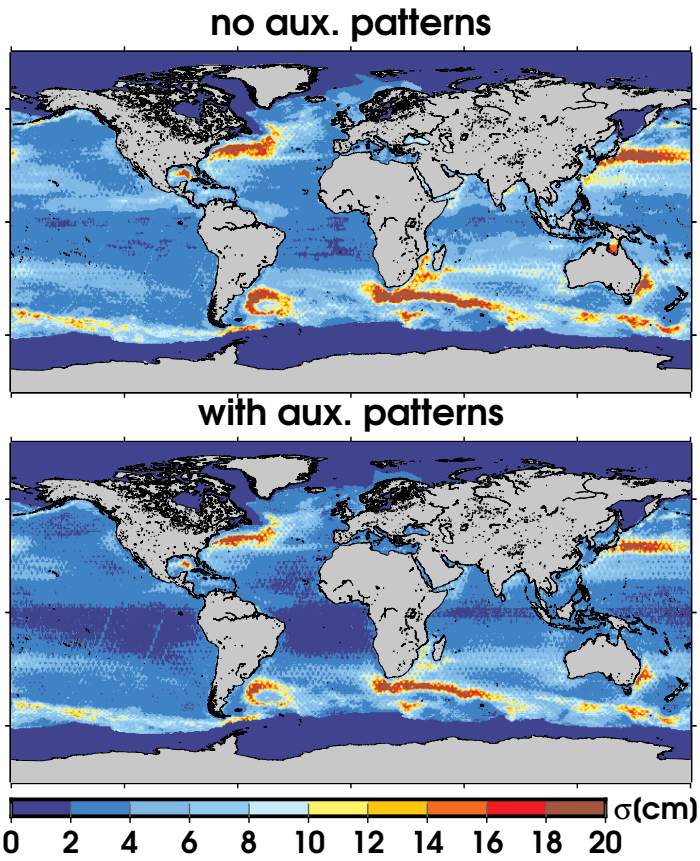

Figure S2: Standard deviation of the altimetry residuals from an inversion without auxiliary patterns (top), and residuals from an inversion using 100 auxiliary patterns(bottom).

model ones, and are in some cases even closer to the PC's from the Ishii data. In conclusion, it seems that the inversion scheme is very forgiving with regards to imperfections in the ocean model.

Stabilization of the Solution

When some patterns (i.e. columns) in matrix **B**, **C** or **D** (see equations 1 and 2 of the main paper) are very similar a (near) rank defect occurs in the normal equation systems. Two such near-rank defects play a role in the inversion. These are mitigated by adding additional constraints to the solution, as described below.

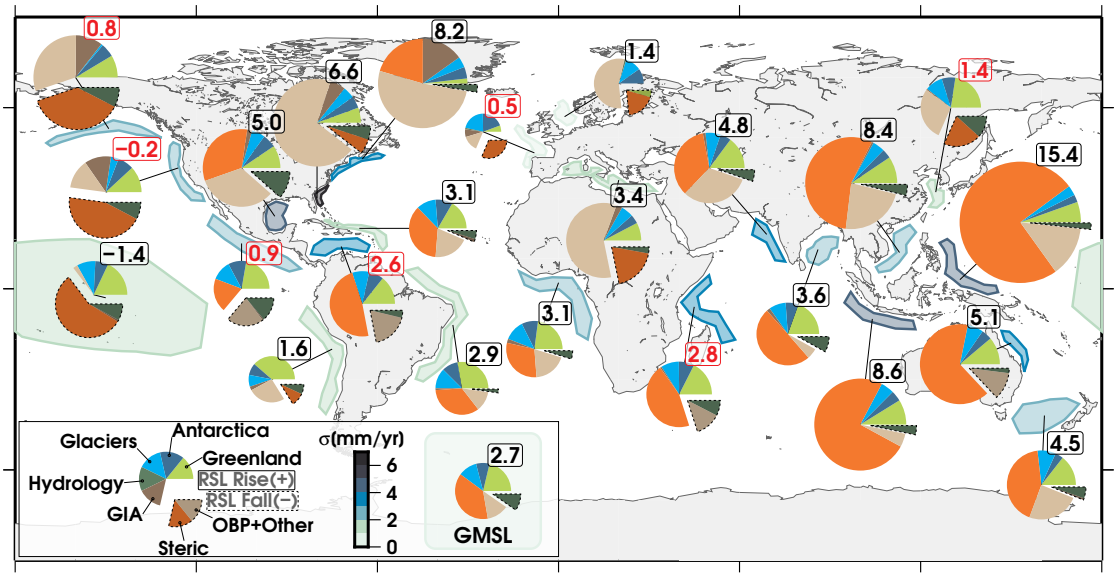

Figure S3: As in Figure 2 of the main article, but the steric fingerprints are now the first 200 leading EOFs of the steric heights from the top 1500m of the Ishii data. In addition, a new set of 100 auxiliary patterns have been computed from the smoothed altimetry residuals as well. Note that the computed total trends have changed, but only within the errorbars.

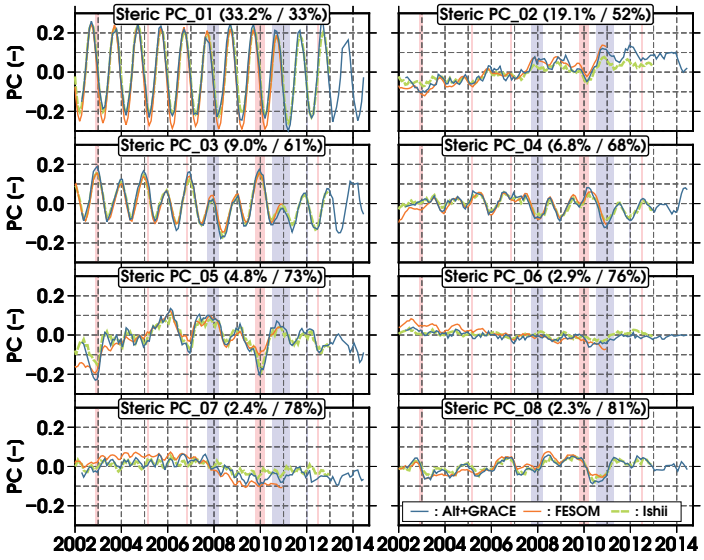

Figure S4: Estimated and computed time series of the first 8 principal components of global steric sea level. The percentages denote how much variance of the FESOM model is explained by the mode (first value indicates %per mode, second value is the cumulative percentage). The curves from the Ishii data are constructed by projecting the computed steric heights onto the modes.

The delineation of some of the basins in Greenland and Antarctica may be too fine to be resolved by the GRACE data, which can only detect signals with large spatial scales (in the order of 100's of km). Within the inversion scheme, the resolving of small basins, particular those which are elongated in north-south direction, therefore introduces strong correlations in some of the estimated ice-sheet parameters[13]. To mitigate this, a constraint has been applied, which penalizes differences between the 20 most sensitive basin combinations in Greenland and Antarctica [1].

A second near-rank defect is caused by the separation of the GIA signal from the overlying mass changes in Greenland and Antarctica. In particular, the fingerprints of the West-Antarctic drainage basins are highly correlated with the Antarctic GIA fingerprint. Recent efforts to separate the GIA signal from present day mass loss in the West Antarctic, exploit a priori information to stabilize the inversion [14]. Here, we have applied a Tikhonov constraint to the GIA parameters. In terms of the normal matrix trace, the constraint determines about 40% and the data the remaining 60% of the GIA parameters. The estimated GIA parameters and effect on sea level are tabulated in table S1 and S2. Interesting is

Table S1: Estimated GIA signal in terms of percentage of the a priori GIA model (based on VM-2 and ICE-5G). 100% means that the estimated GIA component equals the a priori GIA model. The last column describe smaller glacial masses falling outside the major glacial domes.

Laurentide	Antarctica	Fennoscandia	Greenland	other
109%	18%	63%	77%	100%

Table S2: Change in global ocean mean mass contributions (in mm/yr) due to the GIA update compared to using the a priori GIA model

Antarctica	Greenland	Glaciers	Hydrology	Total
-0.223	-0.003	-0.022	0.049	-0.197

that the GIA signal in the Antarctic represents only 18% of the a priori model. This can be partly explained by assuming relatively low upper mantle viscosities in Antarctica as discussed in [15, 16] It is also consistent with the findings from [14].

Comparison with Published Mean Sea Level Budgets

Several other studies exist which provide different estimates of the sea level budget and/or some of its components. Although the total sea level rise agrees to a large extent, the mass component of sea level differs by a fair amount among the studies. Consequently, the derived steric rates will also be affected. Besides the chosen processing methods, there are several other factors which may all contribute to some extent to the estimated mass rates[9]. These range from GIA corrections, geocenter motion corrections, to the chosen time frame. For completeness, we have tabulated some results from other studies in Table S3. Values which agree within the errorbars with our results are highlighted in bold. Although the total sea level, as measured by altimetry, agree well between the studies, there remain several large discrepancies, above the error bars, for estimates of the glaciers and ice sheets. In some cases, mass changes are subtracted from altimetry to obtain steric trends. In such studies, uncertainties in mass changes may also propagate to uncertainties in steric sea level.

Other Coastal zones

For all of the considered coastal zones, the time variation of the diffferent components have been plotted for completeness in the figures S5-S8. The trends of the components of the sea level budget (used in fig. 2 of the main paper) are tabulated for each coastal zone in table S3.

Table S3: Comparison of mean sea level rise contributions in mm/yr from other studies. Trends which agree to those from this study within the errorbars are highlighted in bold. [(a)] The hydrological component only includes modelled anthropogenic interventions and does not include climatic fluctuations (see Table 13.1 of IPCC-AR5 WG1).

	Data	Hydr.	Gr+An+Gl	Steric	Total
This Study	GRACE (GFZ), Altimetry (2002-2014)	**-0.29±0.26**	**1.37±0.09**	**1.38 ±0.16**	**2.74±0.58**
Chen et al. [17]	GRACE (CSR), ARGO(2005-2011)	**-0.07±0.32**	1.73±0.28	0.6±0.27	**2.4±0.54**
IPCC AR5 WG1 [18]	various (1993-2010)	0.38±0.12[(a)]	**1.36±0.39**	**1.1±0.3**	**2.8 ±0.55**
Llovel et al.[19]	GRACE (CSR),Altimetry (2005-2013)	2.0±0.1		0.77±0.28	**2.78±0.32**
Llovel et al. [20]	GRACE (2002-2009)	**-0.22±0.05**			
Johnson et al. [21]	GRACE (2003-2012)	1.8±0.17			
Schrama et al. [9]	GRACE (CSR) (2003-2013)		**1.47±0.09**		
Jensen et al. [22]	GRACE (GFZ), Altimetry (2002-2009)	**-0.2±-0.04**			
Jacob et al.[23]	GRACE (CSR),(2003-2010)		**1.48±0.26**		
Riva et al. [24]	GRACE (DMT) (2003-2009)	**-0.1±0.3**	**1.1±0.2**		
Cazenave et al. [25]	GRACE, Altimetry, ARGO, modelling, etc (2003-2007)	**-0.2±0.1**	1.0±0.2	0.25±0.8	**2.5±0.4**
Dieng et al. [26]	Various T/S data and GRACE (2003-2012)	1.7±0.1		0.56±0.14	**2.82±0.1**

Table S4: Trend of the sea level budget components in mm/yr for the coastal zones considered. Errors are based upon autoregressive models of order 1 which are fitted to the post fit residuals. An exception is the GIA component, which indicate a worst-case scenario error (see the Methods and Materials of the main paper). Gray and black bold values indicate trends which are significant at the 1-σ and 2-σ level respectively.

	Total	Green.	Ant.	Glac.	Hydr.	Steric	OBP+Other	GIA
Africa(East)	2.4 (± 4.16)	**0.8 (± 0.02)**	**0.4 (± 0.06)**	**0.4 (± 0.07)**	**-0.3 (± 0.23)**	0.6 (± 1.90)	0.6 (± 0.91)	0.0 (± 0.16)
Africa(West)	**3.2 (± 2.05)**	**0.8 (± 0.02)**	**0.3 (± 0.06)**	**0.4 (± 0.07)**	-0.1 (± 0.25)	**1.9 (± 1.65)**	-0.1 (± 1.72)	0.1 (± 0.17)
Arabian Sea	**4.6 (± 2.39)**	**0.8 (± 0.02)**	**0.3 (± 0.05)**	**0.4 (± 0.06)**	**-0.3 (± 0.25)**	**4.4 (± 1.69)**	-1.0 (± 2.68)	0.1 (± 0.19)
Australia(East)	**4.8 (± 3.58)**	**0.8 (± 0.02)**	**0.3 (± 0.05)**	**0.4 (± 0.07)**	-0.1 (± 0.27)	**4.8 (± 3.03)**	-1.4 (± 2.71)	0.0 (± 0.20)
Bengal Bay	**3.8 (± 3.26)**	**0.8 (± 0.02)**	**0.3 (± 0.05)**	**0.4 (± 0.07)**	**-0.3 (± 0.27)**	1.5 (± 3.93)	**1.1 (± 0.67)**	0.1 (± 0.22)
Caribbean(East)	**3.5 (± 3.22)**	**0.6 (± 0.02)**	**0.3 (± 0.06)**	**0.4 (± 0.07)**	-0.2 (± 0.18)	0.7 (± 1.63)	1.7 (± 2.74)	-0.1 (± 0.21)
Caribbean Sea	2.0 (± 3.14)	**0.7 (± 0.02)**	**0.3 (± 0.06)**	**0.4 (± 0.07)**	-0.2 (± 0.24)	0.8 (± 2.28)	-0.0 (± 3.54)	-0.0 (± 0.24)
Central America	1.0 (± 2.03)	**0.8 (± 0.02)**	**0.4 (± 0.06)**	**0.4 (± 0.07)**	**-0.5 (± 0.26)**	-0.9 (± 2.20)	0.9 (± 1.85)	-0.0 (± 0.18)
Central Pacific	-1.4 (± 1.42)	**0.9 (± 0.02)**	**0.3 (± 0.06)**	**0.4 (± 0.07)**	**-0.4 (± 0.30)**	**-2.8 (± 1.53)**	0.2 (± 0.52)	-0.0 (± 0.10)
East China Sea	1.3 (± 1.39)	**0.9 (± 0.02)**	**0.3 (± 0.05)**	**0.4 (± 0.06)**	**-0.4 (± 0.27)**	0.0 (± 0.78)	0.2 (± 1.68)	0.0 (± 0.22)
Europe(Atlantic)	**1.0 (± 0.64)**	**0.1 (± 0.01)**	**0.3 (± 0.05)**	**0.3 (± 0.06)**	0.0 (± 0.24)	-0.5 (± 1.27)	**0.7 (± 0.66)**	0.1 (± 0.25)
Gulf of Mexico	**5.9 (± 4.40)**	**0.6 (± 0.02)**	**0.4 (± 0.07)**	**0.4 (± 0.07)**	**-0.7 (± 0.27)**	**2.2 (± 2.01)**	2.9 (± 4.41)	0.1 (± 0.22)
Indonesia	**8.3 (± 4.69)**	**0.8 (± 0.02)**	**0.3 (± 0.06)**	**0.4 (± 0.07)**	**-0.3 (± 0.27)**	**6.4 (± 3.18)**	0.5 (± 0.94)	-0.0 (± 0.21)
Mediterranean	**3.6 (± 1.83)**	**0.5 (± 0.01)**	**0.2 (± 0.05)**	**0.3 (± 0.06)**	-0.2 (± 0.21)	0.6 (± 1.69)	2.0 (± 3.99)	0.2 (± 0.24)
North Sea	**1.4 (± 1.37)**	**-0.1 (± 0.01)**	**0.3 (± 0.05)**	**0.3 (± 0.06)**	0.0 (± 0.24)	-0.3 (± 0.50)	**1.2 (± 0.97)**	0.0 (± 0.36)
Pacific(North)	0.6 (± 4.31)	**0.7 (± 0.02)**	**0.4 (± 0.08)**	0.1 (± 0.08)	**-0.6 (± 0.26)**	**-2.3 (± 1.38)**	**1.6 (± 0.63)**	**0.8 (± 0.28)**
Philippines	**14.7 (± 4.39)**	**0.9 (± 0.02)**	**0.3 (± 0.06)**	**0.4 (± 0.07)**	-0.3 (± 0.26)	**11.2 (± 3.58)**	2.2 (± 2.48)	-0.0 (± 0.17)
South China Sea	**7.6 (± 3.17)**	**0.9 (± 0.02)**	**0.3 (± 0.05)**	**0.4 (± 0.07)**	**-0.3 (± 0.27)**	**5.8 (± 2.41)**	0.5 (± 1.04)	0.1 (± 0.17)
SthAmerica(East)	**3.1 (± 1.57)**	**0.8 (± 0.02)**	**0.3 (± 0.05)**	**0.4 (± 0.07)**	-0.1 (± 0.28)	**1.6 (± 0.98)**	0.1 (± 1.73)	0.0 (± 0.09)
SthAmerica(West)	**1.7 (± 1.56)**	**0.9 (± 0.02)**	**0.2 (± 0.04)**	**0.2 (± 0.06)**	-0.1 (± 0.24)	-1.1 (± 1.62)	**1.6 (± 0.35)**	0.1 (± 0.10)
Tasman Sea	**3.8 (± 0.86)**	**0.7 (± 0.02)**	**0.2 (± 0.04)**	**0.4 (± 0.08)**	-0.3 (± 0.29)	**1.6 (± 1.33)**	**1.1 (± 0.89)**	-0.0 (± 0.23)
US(East)	**6.7 (± 3.85)**	**0.5 (± 0.01)**	**0.4 (± 0.07)**	**0.4 (± 0.07)**	**-0.4 (± 0.29)**	1.8 (± 2.11)	**3.6 (± 2.57)**	**0.5 (± 0.25)**
US(NorthEast)	**9.1 (± 1.72)**	**0.2 (± 0.01)**	**0.4 (± 0.06)**	**0.3 (± 0.07)**	**-0.2 (± 0.22)**	**1.8 (± 1.60)**	**5.3 (± 2.62)**	**1.3 (± 0.25)**
US(West)	-0.3 (± 2.52)	**0.7 (± 0.02)**	**0.4 (± 0.08)**	**0.2 (± 0.07)**	**-0.4 (± 0.24)**	**-2.0 (± 1.49)**	0.2 (± 2.15)	**0.7 (± 0.16)**

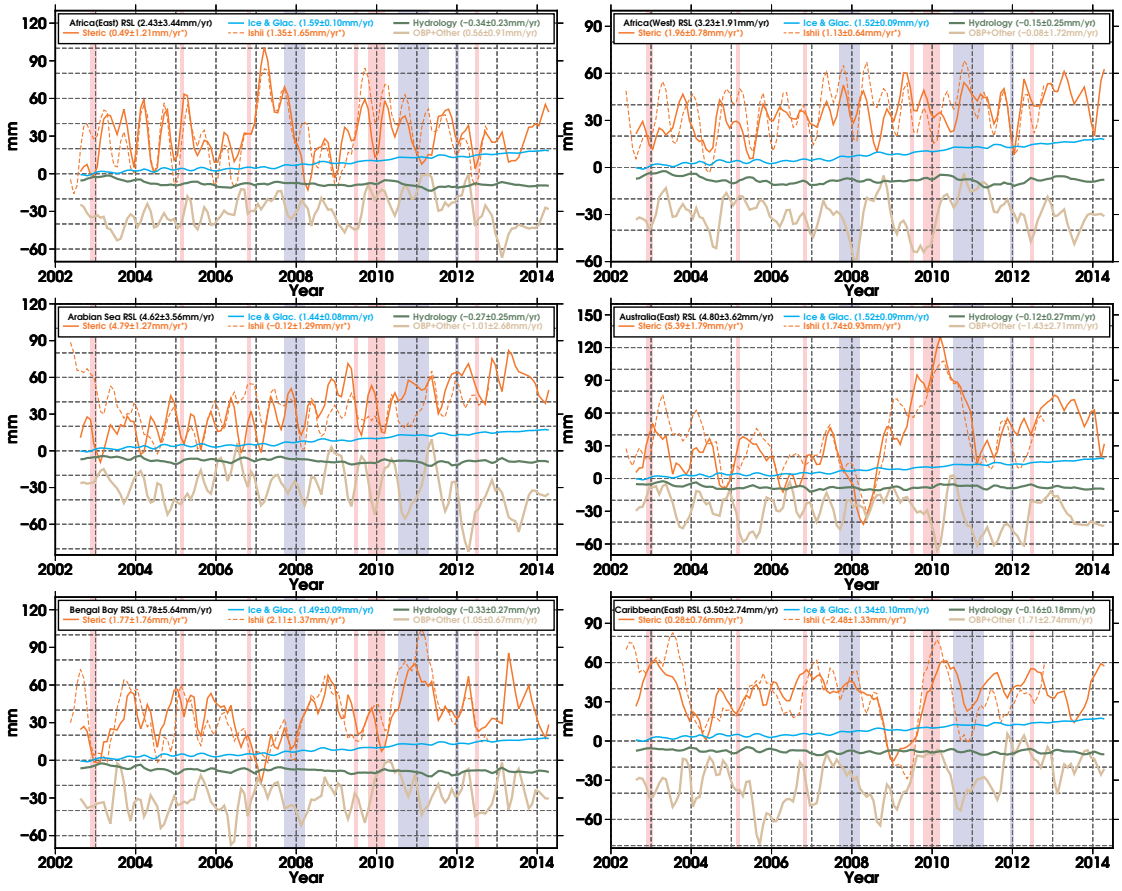

Figure S5: Time variable sea level contributions for varying coastal regions. Warm (El Niño, red) and cold (La Niña, blue) phases are highlighted, whenever the Multivariate ENSO Index (MEI) gets larger than 1 or smaller than -1 respectively. Trends with an asterisk indicate that they are computed over the period where Ishii data is available (2002-2012).

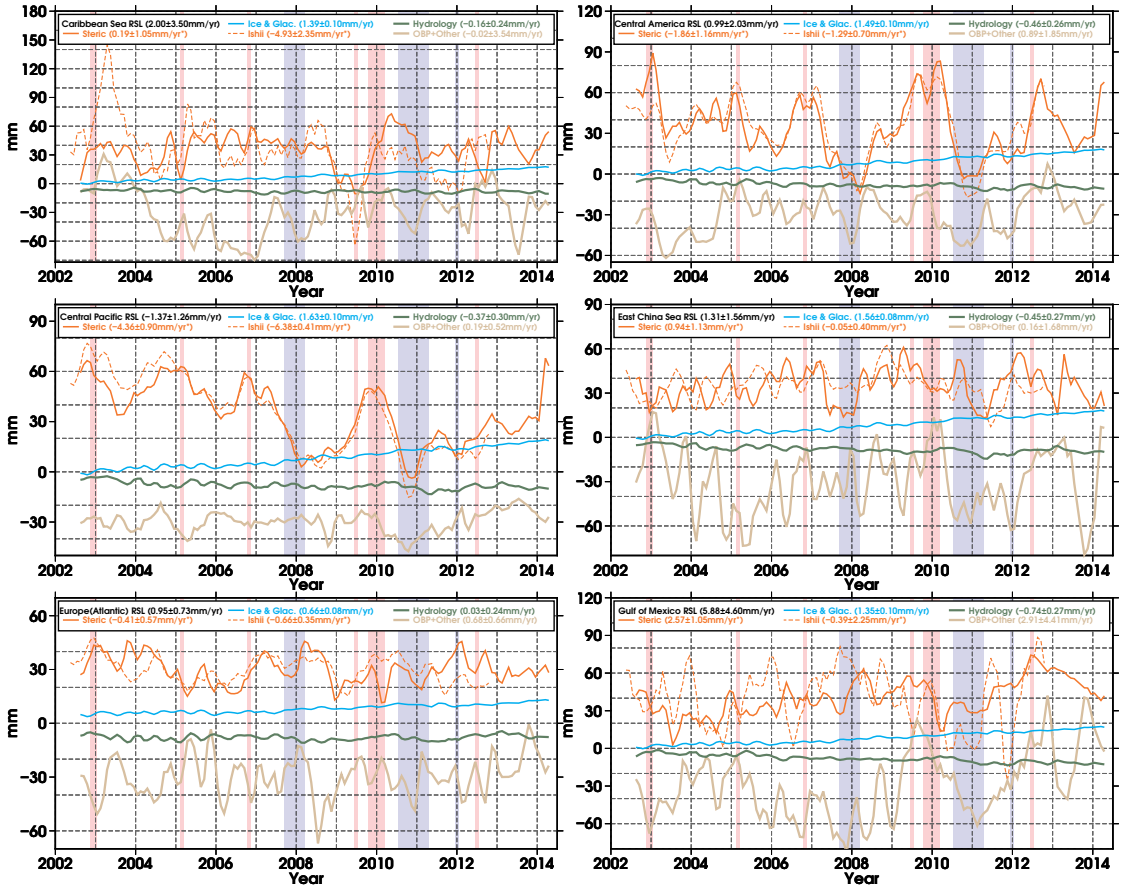

Figure S6: As in Fig. S5 but for various additional regions

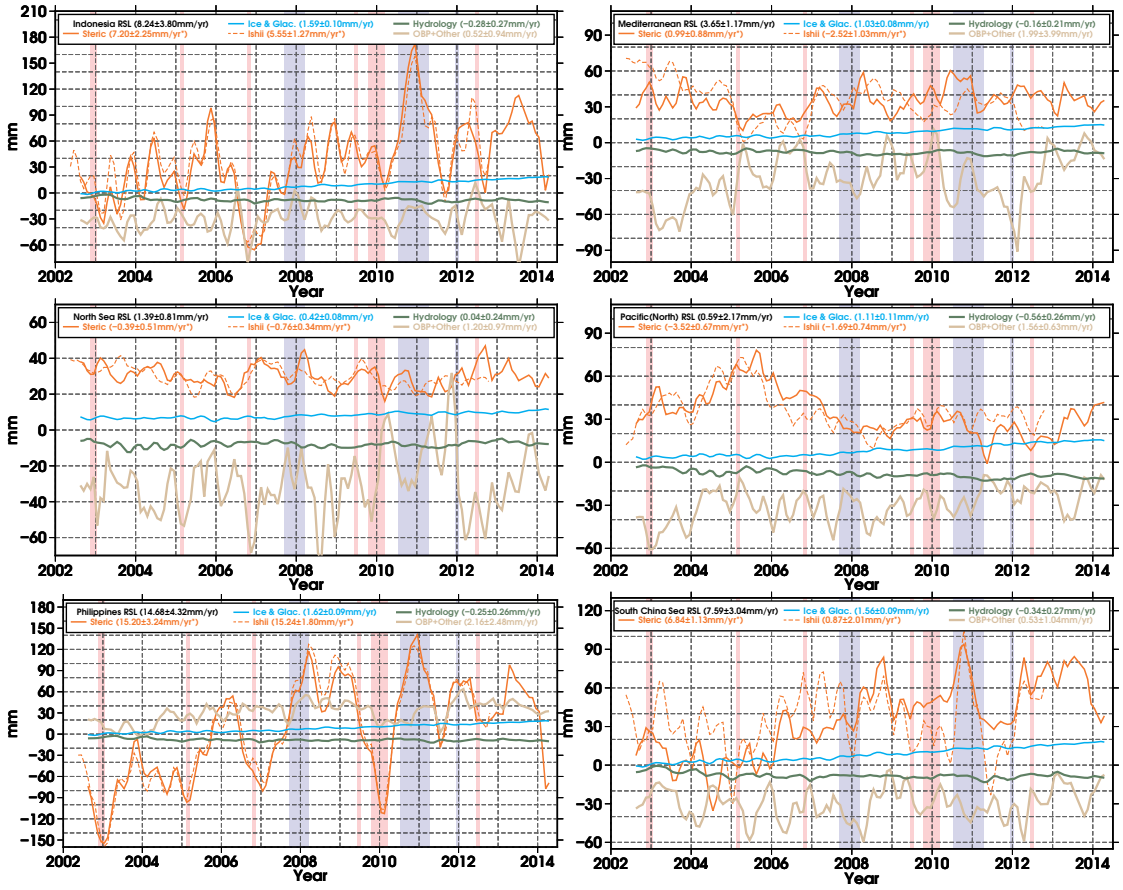

Figure S7: As in Fig. S5 but for various additional regions

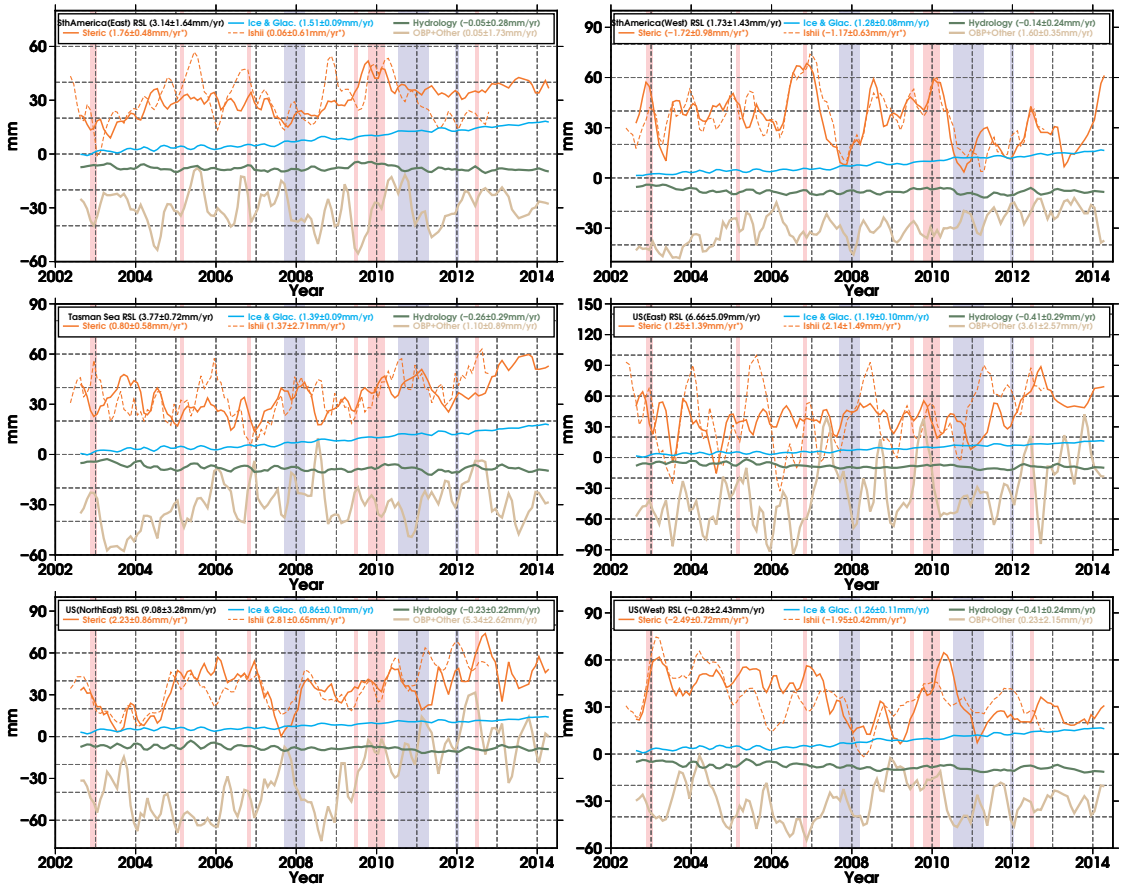

Figure S8: As in Fig. S5 but for various additional regions

References

[1] Rietbroek, R. (2014) Ph.D. thesis (Institute of Geodesy and Geoinformation, Faculty of Agriculture, University of Bonn).

[2] Koch, K.-R. (1988) *Parameter estimation and hypothesis testing in linear models*. (Springer-Verlag New York, Inc.).

[3] Förstner, W. (1979) Ein verfahren zur schätzung von varianz-und kovarianzkomponenten. *Allgemeine Vermessungsnachrichten* **86**, 446–453.

[4] Wouters, B, Chambers, D, & Schrama, E. J. O. (2008) Grace observes small-scale mass loss in greenland. *Geophysical Research Letters* **35**, L20501.

[5] Zwally, H & Giovinetto, M. (2011) Overview and assessment of antarctic ice-sheet mass balance estimates: 1992–2009. *Surveys in Geophysics* **32**, 351–376.

[6] Dahlen, F. A. (1976) The passive influence of the oceans upon the rotation of the earth. *Geophysical Journal of the Royal Astronomical Society* **46**, 363–406.

[7] Raup, B, Racoviteanu, A, Khalsa, S, Helm, C, R, A, & Arnaud, Y. (2007) The glims geospatial glacier database: A new tool for studying glacier change. *Global and Planetary Change* **56**, 101.

[8] Döll, P, Kaspar, F, & Lehner, B. (2003) A global hydrological model for deriving water availability indicators: model tuning and validation. *Journal of Hydrology* **270**, 105–134.

[9] Schrama, E, Wouters, B, & Rietbroek, R. (2014) A mascon approach to assess ice sheet and glacier mass balances and their uncertainties from grace data. *Journal of Geophysical Research: Solid Earth* **119**, 6048âĂŞ6066.

[10] Klemann, V & Martinec, Z. (2011) Contribution of glacial-isostatic adjustment to the geocenter motion. *Tectonophysics* **511**, 99–108.

[11] Peltier, W. (2004) Global glacial isostasy and the surface of the ice-age earth: The ice-5g (vm2) model and grace. *Annual Review of Earth and Planetary Sciences* **32**, 111.

[12] Ishii, M & Kimoto, M. (2009) Reevaluation of historical ocean heat content variations with time-varying xbt and mbt depth bias corrections. *Journal of Oceanography* **65**, 287–299.

[13] Rietbroek, R, Brunnabend, S. E, Kusche, J, & Schröter, J. (2012) Resolving sea level contributions by identifying fingerprints in time-variable gravity and altimetry. *Journal of Geodynamics* **59**, 72–81.

[14] Schoen, N, Zammit-Mangion, A, Rougier, J. C, Flament, T, Rémy, F, Luthcke, S, & Bamber, J. L. (2015) Simultaneous solution for mass trends on the west antarctic ice sheet. *The Cryosphere* **9**, 805–819.

[15] Sasgen, I, Konrad, H, Ivins, E, Van den Broeke, M, Bamber, J, Martinec, Z, Klemann, V, et al. (2013) Antarctic ice-mass balance 2003 to 2012: regional reanalysis of grace satellite gravimetry measurements with improved estimate of glacial-isostatic adjustment based on gps uplift rates. *The Cryosphere* **7**, 1499–1512.

[16] Whitehouse, P. L, Bentley, M. J, Milne, G. A, King, M. A, & Thomas, I. D. (2012) A new glacial isostatic adjustment model for antarctica: calibrated and tested using observations of relative sea-level change and present-day uplift rates. *Geophysical Journal International* **190**, 1464–1482.

[17] Chen, J, Wilson, C, & Tapley, B. (2013) Contribution of ice sheet and mountain glacier melt to recent sea level rise. *Nature Geoscience* **6**, 549–552.

[18] Stocker, T. F, Qin, D, Plattner, G.-K, Tignor, M, Allen, S. K, Boschung, J, Nauels, A, Xia, Y, Bex, V, & Midgley, P. M. (2013) Climate change 2013: The physical science basis. *Intergovernmental Panel on Climate Change, Working Group I Contribution to the IPCC Fifth Assessment Report (AR5)(Cambridge Univ Press, New York)*.

[19] Llovel, W, Willis, J, Landerer, F, & Fukumori, I. (2014) Deep-ocean contribution to sea level and energy budget not detectable over the past decade. *Nature Climate Change*.

[20] Llovel, W, Becker, M, Cazenave, A, Crétaux, J.-F, & Ramillien, G. (2010) Global land water storage change from grace over 2002–2009; inference on sea level. *Comptes Rendus Geosciences* **342**, 179–188.

[21] Johnson, G. C & Chambers, D. P. (2013) Ocean bottom pressure seasonal cycles and decadal trends from grace release-05: Ocean circulation implications. *Journal of Geophysical Research: Oceans* **118**, 4228–4240.

[22] Jensen, L, Rietbroek, R, & Kusche, J. (2013) Land water contribution to sea level from grace and jason-1measurements. *Journal of Geophysical Research: Oceans* **118**, 212–226.

[23] Jacob, T, Wahr, J, Pfeffer, W, & Swenson, S. (2012) Recent contributions of glaciers and ice caps to sea level rise. *Nature*.

[24] Riva, R. E. M, Bamber, J. L, Lavallée, D. A, & Wouters, B. (2010) Sea-level fingerprint of continental water and ice mass change from grace. *Geophysical Research Letters* **37**, L19605.

[25] Cazenave, A & Llovel, W. (2010) Contemporary sea level rise. *Annual Review of Marine Science* **2**, 145–173.

[26] Dieng, H. B, Palanisamy, H, Cazenave, A, Meyssignac, B, & von Schuckmann, K. (2015) The sea level budget since 2003: Inference on the deep ocean heat content. *Surveys in Geophysics* **36**, 209–229.